Visualization and Manipulation of Individual Dopant States in Single Conjugated Oligomers

Shiyong Wang, Weihua Wang, and Nian Lin*

Department of Physics, The Hong Kong University of Science and Technology, Hong Kong, China

ABSTRACT

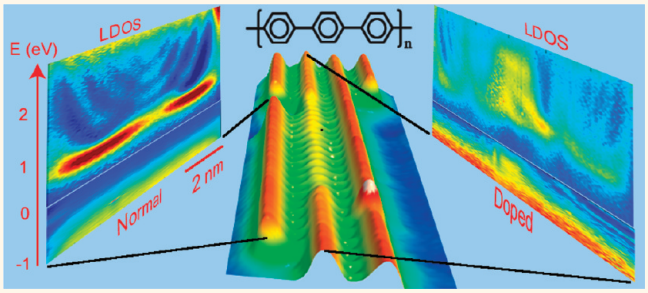

Nonlinear excitations associated with dopant states play fundamental roles for charge transport in conjugated polymers. Here we report on real-space visualization of individual dopant states in single conjugated oligomers of poly-*para*-phenylene using cryogenic scanning tunneling microscopy and spectroscopy. We have found that these states exhibit a typical spatial extension of 4 nm along the oligomers. In particular, these states create a shallow level inside the band gap of the parent oligomers. The origin of these states is traced to a novel doping mechanism of dehydrogenation of the phenylene moiety. Furthermore, we use a scanning tunneling microscope tip to charge/discharge the dopant states and measure their lifetimes. The present results demonstrate a strategy to characterize and manipulate individual dopant states in conjugated polymers with subnanometer resolution.

KEYWORDS: scanning tunneling microscopy · conjugated oligomer · dopant states · single-molecule manipulation

Charge transport in conjugated polymeric chains is formulated in the frame of nonlinear excitations that are introduced through doping.[1−3] The dopant states may enhance charge transport by several orders of magnitude.[1,4,5] In general, these nonlinear excitations create midgap or low-energy states inside the gap of parent polymers, which effectively facilitate the charge transport. The signatures of these midgap states, for example, a reversed spin-charge relationship of the topological soliton, wave function extension, and one-dimensional mobility, have been probed using various experimental techniques.[6−10] However, all the techniques used so far collect an average signal of the ensemble of polymer samples but are unable to provide direct real-space resolution of individual dopant states. This limitation leaves some important issues doubtful or under debate as the ensemble-averaged signals can be misleading.[1] Here we report on real-space visualization of individual dopant states in single conjugated oligomers of poly-*para*-phenylene (PPP) using scanning tunneling microscopy (STM). We find these states are delocalized with a typical spatial extension of ~4 nm where they deform the molecular backbone and significantly alter the electronic characteristics of the parent oligomers, in particular, creating inside the band gap a shallow level. The origin of these states is traced to a novel doping mechanism of dehydrogenation of phenylene. Furthermore, we use STM to charge/discharge the dopant state and measure their lifetime. The present results not only directly verify the predicated signatures of the self-localized excitations but also demonstrate a strategy to characterize and manipulate individual dopant states in conjugated polymers with subnanometer resolution.

RESULTS AND DISCUSSION

STM provides unique opportunities to study single polymers or oligomers owing to its high spatial resolution.[11−14] Figure 1a is an STM image showing PPP oligomers adsorbed on a Cu(111) surface with a typical length over 50 nm, that is, consisting of more than 100 phenyl units. Some oligomers exhibit inhomogeneous topographic height, containing low apparent height (LAH) sections. We examined ~300 such inhomogeneous oligomers and measured the length of the LAH sections. The length distribution statistics drawn in Figure 1b shows that the length falls in a range between 2 and 8 nm while the most popular

* Address correspondence to phnlin@ust.hk.

Received for review January 29, 2012 and accepted March 7, 2012.

Published online March 07, 2012
10.1021/nn300428k

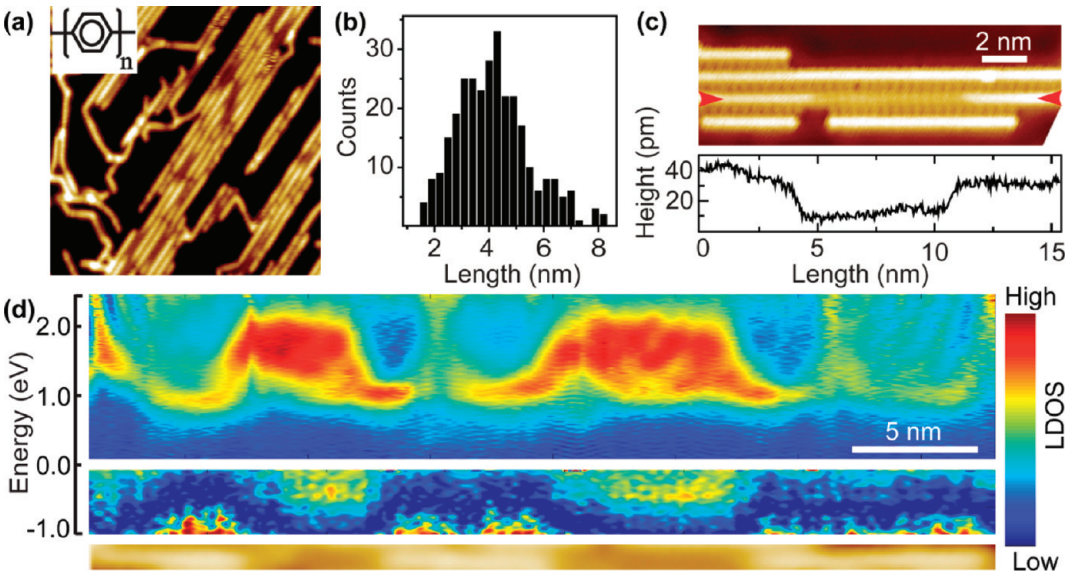

Figure 1. Dopant states in PPP oligomers. (a) STM image (40 × 40 nm^2, 1.0 V, 0.5 nA) showing PPP (inset model) oligomers containing LAH sections adsorbed on a Cu(111) surface. (b) Length distribution of the LAH sections. (c) Top panel: high-resolution STM image (−0.1 V, 0.5 nA) showing a LAH oligomer together with normal ones. Bottom panel: line profile of the LAH oligomer (indicated by red arrows). (d) Spatial map of tunneling spectra (set point, 1.0 V; 0.5 nA; energy is defined with bias voltage) measured along an oligomer showing modified LDOS at two LAH sections (the STM topograph of the oligomer is displayed at the bottom).

length is about 4.5 nm. Figure 1c top panel is a high-resolution STM topograph showing an oligomer containing a LAH section along with several normal ones. The line profile along this oligomer plotted in the low panel of Figure 1c shows the LAH section is ∼20 pm lower than the normal parts of the oligomer (note the normal parts are of the same height as the normal oligomers). As shown later neither the normal nor the LAH sections have an appreciable density of states at the imaging condition of Figure 1c (−0.1 V); the observed height difference is largely due to topographic difference. We thus infer the PPP backbones are deformed at the LAH section. It is worthwhile to note that the height change from the normal section to the LAH section is not an abrupt jump but undergoes a gradual transition in a window of ∼1 nm, indicating that the backbone deformation occurs progressively.

The electronic characteristics of the oligomers containing LAH section are revealed by acquiring spatially resolved d*I*/d*V* tunneling spectra that reflect the local density of states (LDOS).[13] Figure 1d is a spatial LDOS map measured along an oligomer that contains two LAH sections. The normal parts reproduce features of the normal oligomers reported previously,[13] implying the normal parts behave similarly as the normal oligomers. In particular, there is no apparent state appearing between 0.8 and −0.8 eV, which signifies a band gap. In sharp contrast, the two LAH sections exhibit entirely different characteristics: (1) A new state emerges below the Fermi level (around −0.5 eV), that is, inside the gap of the normal oligomers; (2) a set of new states that show very strong intensity in comparison with the conductance band of the normal oligomers lies between 1.0 and 2.0 eV. These new characteristics evidence that the electronic structure of the LAH sections significantly deviates from those of the normal oligomers.

To identify the origin of the LAH sections, we carried out STM manipulation on single oligomers. First, we found the LAH sections can be moved along the oligomers. As shown in Figure 2a, a LAH section was moved ∼3 nm along an oligomer (upwardly) by a voltage pulse applied at the red dot. Second, Figure 2b displays that the oligomer at the left side, which contains a LAH section, was dragged twice on the surface through tip manipulation as marked by the yellow arrows. While the oligomer was displaced, the LAH feature was preserved. These phenomena clearly indicate that the LAH sections are not associated with surface defects underneath the oligomers but rather originate from defects at the oligomer. Next, we found that applying a voltage pulse may create LAH sections in nearby normal oligomers as illustrated in Figure 2c. Note this process is not reversible; an oligomer containing a LAH section cannot be converted into a normal oligomer by bias pulse. It has been reported that voltage pulses applied by STM tip may trigger dehydrogenation of molecular adsorbates.[15] We propose that a similar process occurred here, so, the LAH sections are associated with dehydrogenation defects on the PPP backbones. In the sample preparation, we annealed the samples to different temperatures and found the LAH sections start to appear above 470 K and

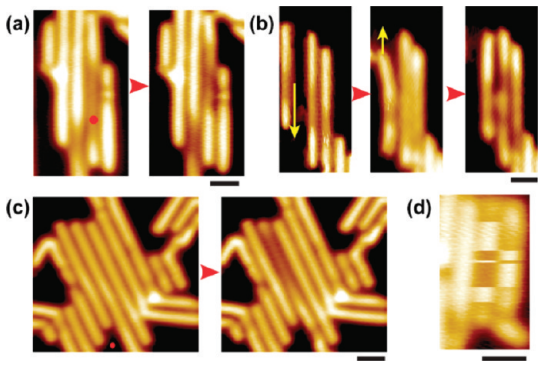

Figure 2. STM manipulation on single oligomers. (a) A LAH section shifts upward after applying a pulse (2.5 V, 10 nA, 0.1 s) at the red dot in the left panel. (b) An oligomer containing a LAH section is displaced twice by tip dragging (as indicated by the yellow arrows). (c) A normal oligomer in the left panel is converted to an oligomer containing LAH in the right panel by a pulse (2.7 V, 30 nA, 0.1 s) applied at the red dot in the left panel. (d) STM image (1.0 V, 0.5 nA) showing the complementary swapping between the middle oligomer and the right one (all scale bars: 2 nm).

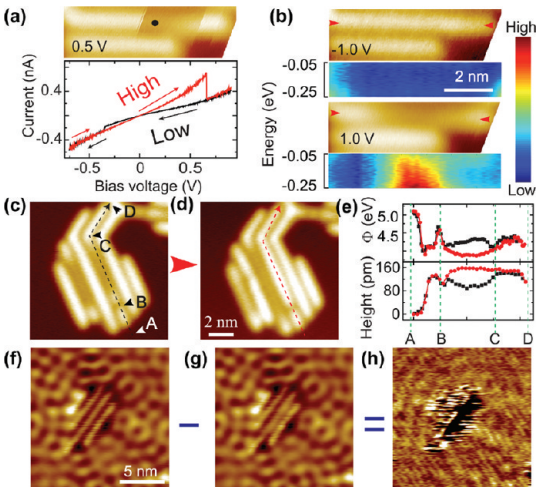

Figure 3. Switching of the dopant states. (a) Top panel: STM image (0.5 V, 0.5 nA) showing an oligomer with abrupt height change (scan direction is parallel to the change lines). Bottom panel: *I*−*V* spectra acquired with the tip positioned above the dot in the top panel. The black and red lines were acquired with decreasing and increasing bias voltage, respectively, as indicated by the arrows. (b) Same area as panel a scanned at bias voltage of −1.0 V (top panel) and 1.0 V (bottom panel), respectively. LDOS plots of the switched oligomer (as marked by red arrows) show that the shallow state appears in the LAH state. (c and d) STM images (1.0 V, 0.5 nA) showing interchain swapping by tip-induced manipulation. (e) Bottom frame: STM topographic height profiles along the dashed lines before (in black) and after (in red) the manipulation. Top frame: spatial resolved work function measured before (in black) and after (in red) the manipulation. (f and g) Surface-state electron wave scattered by three oligomers before and after switching the middle oligomer (0.01 V, 0.5 nA). (h) Differential image of subtracting wave g from wave f.

become more and more abundant with higher temperature annealing. The thermal dehydrogenation of aromatic systems adsorbed on a metallic substrate has been reported previously.[14] These reactions normally occur at a higher temperature.[16] Interestingly, it was reported that dehydrogenation of oligo-phenylenes becomes more appreciable with an increase in the number of phenylene rings.[17,18] The oilgomers studied here are much longer than the molecules addressed previously, so the dehydrogenation may take place at a relatively low temperature. Consistent with this trend, we found most LAH sections appear at longer oligomers. The thermal-induced dehydrogenation is directly confirmed by the formation of the Y-shape branched oligomers (see Supporting Information).

Another evidence of dehydrogenation defects is interchain swapping as shown in Figure 2d: the middle and the right oligomers switch their configuration in a highly correlated manner, that is, as the middle one is at the LAH state, the right one is at the normal state and vice versa. The complementary swapping cannot be attributed to a correlated molecular conformation or adsorption configuration change since the nearest-neighboring hydrogen atoms of two adjacent oligomers are ∼7.5 Å apart, which is too large for any intermolecular interaction. Rather, the swapping can be rationalized by an exchange process that occurred between dehydrogenation and normal oligomers as follows: a hydrogen (or proton) of the normal oligomer may jump to the dehydrogenation defect aided by an intermediate Br atom (*cf.* the small dots lying in the gaps between two neighboring oligomers in Figure 1c[14,19]). The back and forth hydrogen (or proton) transfer gives rise to the complementary swapping behavior (detailed discussion in the Supporting Information).

The LAH sections can be switched between a low-conductance state and a high-conductance state reversibly by STM manipulation. An example is illustrated in Figure 3a where an oligomer shows two abrupt height changes while being scanned at 0.5 V. The switching is manifested explicitly in the *I*−*V* characteristics shown in the low panel of Figure 3a. First, the tip was placed at the position marked by the dot in the top panel STM image; then bias voltage sweeps between 0.90 V and −0.75 V were applied to acquire *I*−*V*. Starting from 0.90 V the *I*−*V* curve (in black) follows a low trace and jumps to a high trace at −0.35 V. In the subsequent backward sweeping, the *I*−*V* initially follows the high trace and jumps to the low trace at 0.65 V. This switching behavior clearly signals that the LAH section jumps back and forth between high-conductance and low-conductance configurations.[20] To determine the electronic signatures of the two configurations, we first set the LAH section at the high-conductance configuration and measured its LDOS (Figure 3b top panel); next, we switched it to the low-conductance configuration and carried out the same measurements (Figure 3b bottom panel).

The LDOS maps reveal that the LAH section at the low-conductance configuration exhibits the shallow state, whereas the high-conductance configuration does not have this shallow state. In a controlled experiment, we performed the same STM manipulation on groups of normal oligomers and found that the normal ones do not exhibit such current bistability, which implies that the bistable behavior is associated with the dehydrogenated defects.

The bistability of molecular adsorbates on surfaces has been reported in literature. The switching mechanism includes molecular conformational interconversion,[21] molecular rotation,[22] hydrogen taotomerization[23] and bistable charge states.[24,25] Among these processes, only the charge bistability manifests that the two states possess distinctive molecular DOS. As revealed in Figure 3b, the high-conductance and the low-conductance states exhibit distinctive molecular DOS, hinting that the observed reversible switching is related to a charge bistability. (Chemical bonding of the dehydrogenated site with the substrate atom is ruled out since such species exhibit very different characteristics. See detailed discussion in Supporting Information.) The charging of organic molecules that are physisorbed on a metallic substrate is very rare as charge is effectively screened by the substrate electrons. Note the charge bistable molecules presented in ref 24 and 25 are adsorbed on an insulating film. Here the PPP oligomers are directly adsorbed on the Cu surface, so, the charging of PPP is unlikely. However, dehydrogenated molecular spices can be stabilized in a charged state as adsorbed on a metallic surface.[26] As discussed previously, it is the dehydrogenated but not the normal oligomers that undergo the reversible switching, signifying the charge bistability only takes place on the oligomers that contain dehydrogenated defects. To verify the proposed charging mechanism, we measured the work function of the oligomers. The low panel in Figure 3e shows the STM topographic height along an oligomer marked by the dashed lines in Figure 3 panels c and d. One can see that the section between points B and C is switched from the low-conductance state to the high-conductance state by a tip manipulation. The top panel in Figure 3e displays the spatial resolved work function measured along the dashed lines before (in black) and after (in red) the manipulation. One can see the two curves reproduce each other between panels A and B, also between panels C and D, where the oligomer is not changed by the manipulation. Interestingly, between panels B and C the work function of the low-conductance state is higher than that of the high-conductance state. It is known that work function of a metal surface is enhanced by an induced dipole of negatively charged molecular adsorbates.[27,28] So, the work function enhancement of the LAH section provides a direct evidence that the LAH sections are negatively charged.

The surface electron wave pattern scattered by the oligomers also support the charging of the LAH oligomers. Figure 3 panels f and g show surface-state waves acquired under the identical parameters around a group of three oligomers. The oligomer in the middle was manipulated at the low-conductance state when acquiring Figure 3f and switched to the high-conductance state when acquiring Figure 3g (note the two side oligomers were unchanged). Figure 3h is obtained by subtracting Figure 3f from 3g. The subtraction excludes all other influences but only conceives the effects of the switching. For example, only the switched oligomer appears as a dark depression in Figure 3h. The most significant feature of Figure 3h is that the subtracted surface state displays ring-like standing wave patterns surrounding the oligomers, which reflects the different scattering strength of the LAH section.[25,29,30]

In chemical terms, a dehydrogenated defect creates a free radical and the negative charging may generate a charged soliton.[1] It is well-known that charge storage in conjugated polymers leads to nonlinear excitations (soliton, polaron, or bipolaron) that have delocalized spin or charge distributions.[1] The LAH sections exhibit several key characteristic signatures of the nonlinear excitations in 1D conjugated polymer: First, the STM-resolved structural deformation is in consistent with the predicated structural relaxation associated with the nonlinear excitations. In particular, it was predicted that negatively charged PPP takes on a planar structure,[31] which corroborates the observed LAH feature. Second, theory predicted solitons in polyacetylene or polarons in poly-phenylene-vinylene extend over eight monomer units.[32,33] The typical depression length of ~4.5 nm (10 phenylene units) agrees well with the predications. In addition, we found that once a switching occurred, entire LAH sections were switched, which indicates the LAH sections are entities that extend along the oligomers. Third, the in-gap level as revealed by LDOS may correspond to the shallow states or midgap state associated with the nonlinear excitons. At the experimental temperature of 5 K, the LAH sections are immobile. Nevertheless, the voltage-pulse induced motion as illustrated in Figure 2a hints that these dopant states may become mobile with sufficient energy. Unlike normal electron or hole doping of PPP which results in polaron or bipolaron, the dehydrogenation somehow resembles an inverse process of the protonation doping of polyaniline.[1,4,5] It is worthwhile to point out that the spatial extension and the shallow in-gap level suggest that these dopants may effectively enhance the conductivity of PPP or other types of phenylene-based polymers.

In the following, we present detailed analysis of the rates of single-chain switching and interchain swapping. In 0.1 V STM imaging (left panel in Figure 4a), the

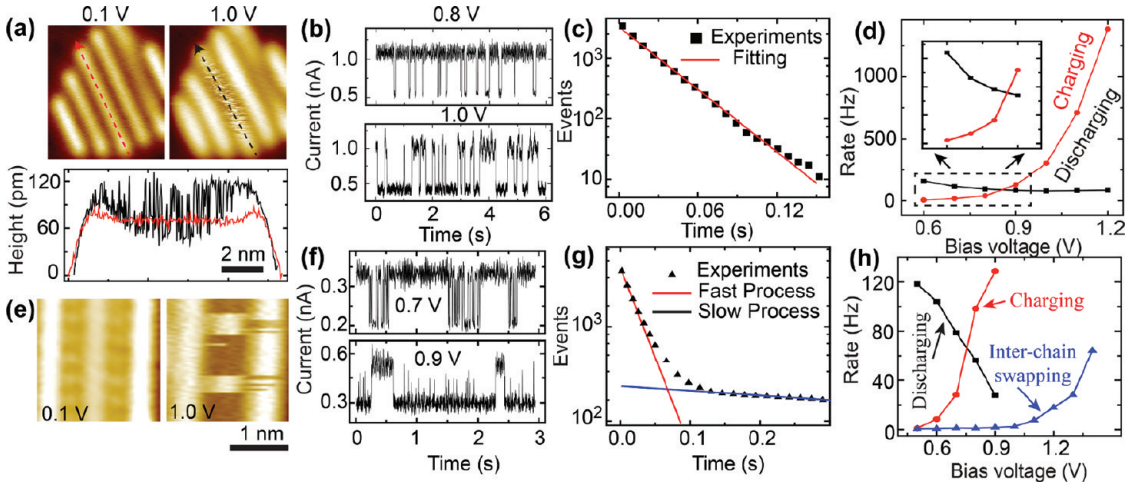

Figure 4. Manipulating the charging states of the dopant states. (a–d) Switching of single oligomers: (a) top panel, STM images acquired at bias of 0.1 and 1.0 V; bottom panel, line profiles of the oligomer marked by red and black arrows. (b) *I*–*t* traces acquired at bias of 0.8 and 1.0 V. (c) Exponential decay of high-state events as a function of resident time at 0.8 V. (d) Switching rate in the high-conductance state (red), and in the low-conductance state (black) as a function of bias voltage. (e–h) Interchain swapping: (e) left panel, STM images acquired at 0.1 and 1 V. The dot-like features between two oligomers are bromine atoms. (f) *I*–*t* traces acquired at bias of 0.7 and 0.9 V. (g) Double-exponential decay of high-state events as a function of resident time at 0.7 V. (h) Switching rate of charging, discharging, and interchain swapping as a function of bias voltage.

oligomer marked by the red line appears as a normal one, while in 1.0 V imaging (right panel) the same oligomer appears very noisy. This unstable behavior indicates that the oligomer experiences a fast switching process at 1.0 V. To determine the switching rate, we monitored the current over a period of time (*I*–*t*) under fixed tunneling conditions. Two *I*–*t* traces acquired at bias voltages of 0.8 and 1.0 V shown in Figure 4b reveal in both cases the current jumps between a high state and a low state. According to the previous discussion, the high/low state corresponds to the neutral/negatively charged state of a radical oligomer. So, the fast switching manifests a fast charging–discharging process. The two *I*–*t* traces behave differently: the current resides longer at the high state at 0.8 V but shorter at 1.0 V, suggesting the charging–discharging process is bias-voltage dependent. Figure 4c displays the number of events that continuously rest at the high state for certain duration (defined as resident time) decays exponentially as a function of the resident time. The slope of this exponential function defines the charging rate or inverse of the neural state lifetime.[22,34] As summarized in Figure 4d, the charging rate increases exponentially with respect to the increasing bias voltage, whereas the discharging rate decreases slightly with respect to the bias voltage. This behavior indicates the charging and discharging must obey different mechanisms: As the discharging mostly depends on the adsorption configuration, not the energy of the tunneling electrons, the discharging rate is not very sensitive to the bias voltage. In contrast, the charging is a process closely related to the energy of the tunneling electrons so the charging rate is enhanced dramatically at higher bias voltages.

The left panel in Figure 4e is a STM topography imaged at 0.1 V showing two normal oligomers and one LAH oligomer (middle). The 1.0 V STM imaging (right panel) reveals the middle and the right oligomers swap their configurations. Two *I*–*t* traces (Figure 4f) obtained by positioning the tip above one of the swapping oligomers exhibit similarly two-level switching but with a new character: when the current is at the low state, many short-life switching events (shown by the spikes in the *I*–*t* traces) occur; in contrast, when the current is at the high state, such short-life switching disappears. This new behavior becomes evident in Figure 4g which shows the switching no longer obeys a simple exponential decay, but rather exhibits two decaying slopes. Such a double-exponential decay has been reported in a system associated with two processes with different rate.[35] Here we attribute the fast process to the charging–discharging of single oligomers and the slow process to interchain hydrogen transfer (note in some scan lines of the 1.0 V image in Figure 4e both oligomers appear in the high state. This corresponds to a situation that one oligomer is normal while the other is dehydrogenated but not negatively charged). Figure 4h displays the bias–voltage dependent switching rates: the rate of hydrogen transfer becomes apparent above 1.1 V, while the charging/discharging rate follows the same trends as in the single-oligomer switching (*cf.* Figure 4d).

CONCLUSIONS

We immobilized the dopant states in conjugated oligomers at a cryogenic temperature of 5 K and used high-resolution STM to examine individual dopant states. Our data, for the first time to our

knowledge, directly reveal (1) the characteristic spatial extension of the dopant states, (2) molecular backbone structural deformation, and (3) a localized shallow level within the energy gap of the undoped parent oligomers. These results provide deep insights into the physics and chemistry of conducting conjugated polymers. We believe this study presents a strategy to directly examine and manipulate localized dopant states at single conjugated polymers.

EXPERIMENTAL SECTION

The experiments were carried out in an ultrahigh vacuum scanning tunneling microscope system (Omicron) operated at 4.9 K. A Cu(111) single crystal was cleaned by cycles of Ar ion sputtering and annealing. Molecules of 4,4″-dibromo-*p*-terphenyl (Sigma Aldrich) were thermally degassed and evaporated onto the Cu(111) substrate held at room temperature. This was followed by a 490 K annealing of the substrate to form the PPP oligomers. The STM topography data were acquired in constant current mode. The d*I*/d*V* signals were measured using a lock-in amplifier with a sine modulation of 1.5 kHz and a modulation of 15 mV. In LDOS maps, each d*I*/d*V* spectrum was normalized by (*I*/*V*). The work function data were measured by acquiring *I*−*z* spectra at a specific bias voltage point-by-point along the oligomers (the determined values of work function was found to be independent of set point). The STM tip-drag manipulation was conducted by approaching the tip to the oligomers with a bias voltage of −2 V, and then laterally moving the tip in a designed pathway.

Conflict of Interest: The authors declare no competing financial interest.

Acknowledgment. This work is financially supported by Hong Kong RGC under Grant No. 602409.

Supporting Information Available: Thermal-induced dehydrogenation of PPP phenylene moieties, mechanism of interchain swapping, converting LAH section to a surface-bonded configuration, and switching behavior of LAH oligomers. This material is available free of charge *via* the Internet at http://pubs.acs.org.

REFERENCES AND NOTES

1. Heeger, A. J.; Kivelson, S.; Schrieffer, J. R.; Su, W. P. Solitons in Conducting Polymers. *Rev. Mod. Phys.* **1988**, *60*, 781–850.
2. Bredas, J. L.; Street, G. B. Polarons, Bipolarons, and Solitons in Conducting Polymers. *Acc. Chem. Res.* **1985**, *18*, 309–315.
3. Brazovskii, S.; Kirova, N. Physical Theory of Excitons in Conducting Polymers. *Chem. Soc. Rev.* **2010**, *39*, 2453–2465.
4. Heeger, A. J. Nobel Lecture: Semiconducting and Metallic Polymers: The Fourth Generation of Polymeric Materials. *Rev. Mod. Phys.* **2001**, *73*, 681–700.
5. Heeger, A. J.; Sariciftci, N. S.; Namdas, E. B., *Semiconducting and Metallic Polymers.*: Oxford University Press: Oxford, UK, 2010.
6. Chen, J.; Heeger, A. J. *In situ* Electron-Spin Resonance Experiments on Polyacetylene during Electrochemical Doping. *Synth. Met.* **1988**, *24*, 311–327.
7. Etemad, S.; Pron, A.; Heeger, A. J.; Macdiarmid, A. G.; Mele, E. J.; Rice, M. J. Infrared-Active Vibrational-Modes of Charged Solitons in $(Ch)_X$ and $(Cd)_X$. *Phys. Rev. B* **1981**, *23*, 5137–5141.
8. Miranda, P. B.; Moses, D.; Heeger, A. J.; Park, Y. W. Excitation Spectrum for Ultrafast Photogeneration of Charged Solitons in Polyacetylene. *Phys. Rev. B* **2002**, *66*, 125202.
9. Chen, J.; Heeger, A. J.; Wudl, F. Confined Soliton Pairs (Bipolarons) in Polythiophene—*In situ* Magnetic-Resonance Measurements. *Solid State Commun.* **1986**, *58*, 251–257.
10. Nowak, M. J.; Spiegel, D.; Hotta, S.; Heeger, A. J.; Pincus, P. A. Charge Storage on a Conducting Polymer in Solution. *Macromolecules* **1989**, *22*, 2917–2926.
11. Repp, J.; Liljeroth, P.; Meyer, G. Coherent Electron-Nuclear Coupling in Oligothiophene Molecular Wires. *Nat. Phys.* **2010**, *6*, 975–979.
12. Lafferentz, L.; Ample, F.; Yu, H.; Hecht, S.; Joachim, C.; Grill, L. Conductance of a Single Conjugated Polymer as a Continuous Function of its Length. *Science* **2009**, *325*, 1193–1197.
13. Wang, S.; Wang, W.; Lin, N. Resolving Band-Structure Evolution and Defect-Induced States of Single Conjugated Oligomers by Scanning Tunneling Microscopy and Tight-Binding Calculations. *Phys. Rev. Lett.* **2011**, *106*, 206803.
14. Wang, W.; Shi, X.; Wang, S.; Van Hove, M. A.; Lin, N. Single-Molecule Resolution of an Organometallic Intermediate in a Surface-Supported Ullmann Coupling Reaction. *J. Am. Chem. Soc.* **2011**, *133*, 13264–13267.
15. Zhao, A.; Li, Q.; Chen, L.; Xiang, H.; Wang, W.; Pan, S.; Wang, B.; Xiao, X.; Yang, J.; Hou, J. G.; *et al.* Controlling the Kondo Effect of an Adsorbed Magnetic Ion through Its Chemical Bonding. *Science* **2005**, *309*, 1542–1544.
16. Mullegger, S.; Winkler, A. Hexaphenyl Thin Films on Clean and Carbon Covered Au(111) Studied with TDS and LEED. *Surf. Sci.* **2006**, *600*, 1290–1299.
17. Bayat, M.; Salehzadeh, S. Theoretical Studies on the Proton Affinities of Four Different Series of Nano-size Diamines and Designing Strong Superbases Based on Fullerene(C_{60}) Molecule. *J. Mol. Struct.: THEOCHEM* **2010**, *957*, 120–125.
18. Müllegger, S.; Winkler, A. Dehydrogenation of Oligophenylenes on Gold Surfaces. *Surf. Sci.* **2006**, *600*, 3982–3986.
19. Lipton-Duffin, J. A.; Ivasenko, O.; Perepichka, D. F.; Rosei, F. Synthesis of Polyphenylene Molecular Wires by Surface-Confined Polymerization. *Small* **2009**, *5*, 592–597.
20. Qiu, X. H.; Nazin, G. V.; Ho, W. Mechanisms of Reversible Conformational Transitions in a Single Molecule. *Phys. Rev. Lett.* **2004**, *93*, 196806.
21. Yasuda, S.; Nakamura, T.; Matsumoto, M.; Shigekawa, H. Phase Switching of a Single Isomeric Molecule and Associated Characteristic Rectification. *J. Am. Chem. Soc.* **2003**, *125*, 16430–16433.
22. Stipe, B. C.; Rezaei, M. A.; Ho, W. Inducing and Viewing the Rotational Motion of a Single Molecule. *Science* **1998**, *279*, 1907–1909.
23. Liljeroth, P.; Repp, J.; Meyer, G. Current-Induced Hydrogen Tautomerization and Conductance Switching of Naphthalocyanine Molecules. *Science* **2007**, *317*, 1203–1206.
24. Wu, S. W.; Ogawa, N.; Nazin, G. V.; Ho, W. Conductance Hysteresis and Switching in a Single-Molecule Junction. *J. Phys. Chem. C* **2008**, *112*, 5241–5244.
25. Swart, I.; Sonnleitner, T.; Repp, J. Charge State Control of Molecules Reveals Modification of the Tunneling Barrier with Intramolecular Contrast. *Nano Lett.* **2011**, *11*, 1580–1584.
26. Payer, D.; Comisso, A.; Dmitriev, A.; Strunskus, T.; Lin, N.; Wöll, C.; DeVita, A.; Barth, J. V.; Kern, K. Ionic Hydrogen Bonds Controlling Two-Dimensional Supramolecular Systems at a Metal Surface. *Chem.—Eur. J.* **2007**, *13*, 3900–3906.
27. Bagus, P. S.; Staemmler, V.; Woll, C. Exchangelike Effects for Closed-Shell Adsorbates: Interface Dipole and Work Function. *Phys. Rev. Lett.* **2002**, *89*, 096104.
28. Vitali, L.; Levita, G.; Ohmann, R.; Comisso, A.; De Vita, A.; Kern, K. Portrait of the Potential Barrier at Metal−Organic Nanocontacts. *Nat. Mater.* **2010**, *9*, 320–323.
29. Repp, J.; Meyer, G.; Olsson, F. E.; Persson, M. Controlling the Charge State of Individual Gold Adatoms. *Science* **2004**, *305*, 493–495.

30. Olsson, F. E.; Paavilainen, S.; Persson, M.; Repp, J.; Meyer, G. Multiple Charge States of Ag Atoms on Ultrathin NaCl Films. *Phys. Rev. Lett.* **2007**, *98*, 176803.
31. Imamura, A.; Orimoto, Y.; Aoki, Y. Molecular and Electronic Structures of Bipolaron in Poly-*para*-Phenylene in Terms of Molecular Orbital Symmetry. *Theo. Chem. Acc* **1999**, *102*, 180–187.
32. Rohlfing, M.; Louie, S. G. Optical Excitations in Conjugated Polymers. *Phys. Rev. Lett.* **1999**, *82*, 1959–1962.
33. Su, W. P.; Schrieffer, J. R.; Heeger, A. J. Solitons in Polyacetylene. *Phys. Rev. Lett.* **1979**, *42*, 1698–1701.
34. Wang, W.; Shi, X.; Jin, M.; Minot, C.; Van Hove, M. A.; Collin, J.-P.; Lin, N. Electron Stimulation of Internal Torsion of a Surface-Mounted Molecular Rotor. *ACS Nano* **2010**, *4*, 4929–4935.
35. Stipe, B. C.; Rezaei, M. A.; Ho, W. Localization of Inelastic Tunneling and the Determination of Atomic-Scale Structure with Chemical Specificity. *Phys. Rev. Lett.* **1999**, *82*, 1724–1727.